J|A|C|S
ARTICLES

Published on Web 09/24/2010

# Interaction of Charge Carriers with Lattice Vibrations in Oligoacene Crystals from Naphthalene to Pentacene

Roel S. Sánchez-Carrera,[†,#] Pavel Paramonov,[†,§] Graeme M. Day,[‡] Veaceslav Coropceanu,*[,†] and Jean-Luc Brédas*[,†]

*School of Chemistry and Biochemistry and Center for Organic Photonics and Electronics, Georgia Institute of Technology, 901 Atlantic Drive NW, Atlanta, Georgia 30332-0400, and Department of Chemistry, University of Cambridge, Lensfield Road, Cambridge CB2 1EW, U.K.*

Received May 12, 2010; E-mail: coropceanu@gatech.edu; jean-luc.bredas@chemistry.gatech.edu

***Abstract:*** A key feature of organic $\pi$-conjugated materials is the strong connection between their electronic and geometric structures. In particular, it has been recently demonstrated that nonlocal electron−vibration (electron−phonon) interactions, which are related to the modulation of the electronic couplings (transfer integrals) between adjacent molecules by lattice vibrations, play an important role in the charge-transport properties of organic semiconductors. Here, we use density functional theory calculations and molecular mechanics simulations to estimate the strength of these nonlocal electron−vibration couplings in oligoacene crystals as a function of molecular size from naphthalene through pentacene. The effect of each optical vibrational mode on the electronic couplings is evaluated quantitatively. The results point to a very strong coupling to both *inter*molecular vibrational modes and *intra*molecular (including high-frequency) modes in all studied systems. Importantly, our results underline that the amount of relaxation energy associated with nonlocal electron−phonon coupling *decreases* as the size of the molecule increases. This work establishes an original relationship between chemical structure and nonlocal vibrational coupling in the description of charge transport in organic semiconductor crystals.

## 1. Introduction

The rapid growth in the design and synthesis of new organic semiconductors[1] and their applications in organic (opto)electronic devices[2−7] has revived interest in the theoretical description of charge transport in organic $\pi$-conjugated materials.[8−11] Although several charge-transport theories have been developed,[12−15] reaching a complete understanding of the charge-transport mechanisms in organic crystals still poses a major challenge. A long-standing problem in the development of new transport models comes from the lack of reliable estimates for the microscopic parameters determining the charge-carrier mobilities; this is, in particular, the case for the coupling between the motions of the charge carriers and the intra- and intermolecular vibrations, which can be quantified through the electron−vibration (phonon) coupling constants. (We recall that the phonons represent the vibrational modes in crystalline structures and incorporate the three-dimensional periodicity of the lattice.)

Two major electron−vibration coupling mechanisms can be distinguished in the framework of a simple tight-binding (Hückel-like) description of organic semiconductors. The first comes from the modulation by vibrations of the site energy, $\varepsilon_m$ (or Coulomb integral $\alpha$ in Hückel terminology), and is termed the *local* electron−vibration (phonon) coupling. In a rigorous sense, the site energy corresponds to the energy of the cation [anion] state in the case of a positively [negatively] charged carrier or can be more crudely approximated to the HOMO [LUMO] energy. The local coupling represents a key interaction in Holstein-type polaron models,[16,17] and its strength is expressed by the polaron binding energy, $E_{pol}$; in the context of Marcus electron-transfer theory, the local coupling can actually

[†] Georgia Institute of Technology.
[‡] University of Cambridge.
[#] Present address: Research and Technology Center North America, Robert Bosch LLC, Cambridge, MA 02142.
[§] Present address: Department of Physics, The Ohio State University at Newark, Newark, OH 43055.

(1) Anthony, J. E. *Angew. Chem., Int. Ed.* **2008**, *47*, 452.
(2) Friend, R. H.; Gymer, R. W.; Holmes, A. B.; Burroughes, J. H.; Marks, R. N.; Taliani, C.; Bradley, D. D. C.; Dos Santos, D. A.; Brédas, J. L.; Logdlund, M.; Salaneck, W. R. *Nature* **1999**, *397*, 121.
(3) Garnier, F.; Hajlaoui, R.; Yassar, A.; Srivastava, P. *Science* **1994**, *265*, 1684.
(4) Kim, J. Y.; Lee, K.; Coates, N. E.; Moses, D.; Nguyen, T. Q.; Dante, M.; Heeger, A. J. *Science* **2007**, *317*, 222.
(5) Scharber, M. C.; Wuhlbacher, D.; Koppe, M.; Denk, P.; Waldauf, C.; Heeger, A. J.; Brabec, C. L. *Adv. Mater.* **2006**, *18*, 789.
(6) Tang, C. W. *Appl. Phys. Lett.* **1986**, *48*, 183.
(7) Tang, C. W.; Vanslyke, S. A. *Appl. Phys. Lett.* **1987**, *51*, 913.
(8) Brédas, J. L.; Beljonne, D.; Coropceanu, V.; Cornil, J. *Chem. Rev.* **2004**, *104*, 4971.
(9) Coropceanu, V.; Cornil, J.; da Silva Filho, D. A.; Olivier, Y.; Silbey, R.; Brédas, J. L. *Chem. Rev.* **2007**, *107*, 926.
(10) Grozema, F. C.; Siebbeles, L. D. A. *Int. Rev. Phys. Chem.* **2008**, *27*, 87.
(11) Nelson, J.; Kwiatkowski, J. J.; Kirkpatrick, J.; Frost, J. M. *Acc. Chem. Res.* **2009**, *42*, 1768.
(12) Hannewald, K.; Stojanovic, V. M.; Schellekens, J. M. T.; Bobbert, P. A.; Kresse, G.; Hafner, J. *Phys. Rev. B* **2004**, *69*, 075211.
(13) Kenkre, V. M.; Andersen, J. D.; Dunlap, D. H.; Duke, C. B. *Phys. Rev. Lett.* **1989**, *62*, 1165.
(14) Munn, R. W.; Silbey, R. *J. Chem. Phys.* **1985**, *83*, 1843.
(15) Munn, R. W.; Silbey, R. *J. Chem. Phys.* **1985**, *83*, 1854.
(16) Holstein, T. *Ann. Phys. (N.Y.)* **1959**, *8*, 325.
(17) Holstein, T. *Ann. Phys. (N.Y.)* **1959**, *8*, 343.

  

be expressed by the reorganization energy $\lambda$ (which corresponds to ca. $2E_{pol}$).

The second mechanism is due to the dependence of the transfer integral (electronic coupling), $t_{mn}$ (resonance integral $\beta$ in Hückel terminology), on the distances between adjacent molecules and their relative orientations; it is commonly referred to as *nonlocal* or Peierls-type electron−phonon coupling.[18] While in most recent studies the emphasis was placed on local coupling and the corresponding coupling constants,[9] there is currently a growing consensus that the nonlocal electron−phonon mechanism can also play an important (and, in some cases, even dominant) role. Therefore, it should be properly taken into account when describing the charge-transport properties of organic molecular solids.[12,19−31]

As it turns out, nonlocal electron−phonon interactions have been much less studied than their local counterparts. In fact, a detailed quantum-chemical investigation of the nonlocal electron−phonon coupling has been performed so far only for the naphthalene crystal.[19] In order to evaluate the interaction of charge carriers with optical lattice vibrations in this crystal, we developed an approach that combines the calculation of crystal vibrations (using either density functional theory or molecular mechanics methods) and a numerical derivation of the electron−phonon coupling constants. Here, we extend this approach to the larger members of the oligoacene family: anthracene, tetracene, and pentacene. To the best of our knowledge, this work represents the first investigation of the dependence of the nonlocal electron−phonon interactions *as a function of molecular size* in organic semiconducting crystals and, thus, of their dependence on chemical structure. The results reported here might therefore be expected to bring a significant contribution to our understanding of charge transport in organic semiconductors.

## 2. Methodology

In the tight-binding approximation, the electronic properties of the system are described by the following Hamiltonian:

$$H = \sum_m \varepsilon_m a_m^+ a_m + \sum_{mn} t_{mn} a_m^+ a_n \tag{1}$$

where $a_m^+$ and $a_m$ denote the creation and annihilation operators for an electron at site $m$. The nonlocal electron−vibration interactions are evaluated by expanding the transfer integrals, $t_{mn}$, in a power series of the vibration (phonon) coordinates. Here, we consider the modulations of the transfer integrals by the optical phonons. As has been the case in previous investigations,[12,19,30] the dispersion of the optical modes (that is, the variation of the vibrational modes as a function of momentum in reciprocal space) is neglected, which means that the strengths of the nonlocal electron−phonon interactions are estimated by using the normal-mode coordinates derived at the Γ-point (the center of the Brillouin zone in reciprocal space). The Hamiltonian for the lattice vibrations, $H_L$, and the dependence of the transfer integrals on normal-mode coordinates are given by

$$H_L = \frac{1}{2}\sum_j \hbar\omega_j (P_j^2 + Q_j^2) \tag{2}$$

$$t_{mn} = t_{mn}^{(0)} + \sum_j v_{jmn} Q_j + \cdots \tag{3}$$

Here, $\omega_j$, $Q_j$, and $P_j$ denote the frequency and the dimensionless coordinate and momentum of vibration mode $j$, respectively; the $t_{mn}^{(0)}$ terms denote the transfer integrals between molecules at sites $m$ and $n$ obtained at the equilibrium geometry; the $v_{jmn}$ terms represent the linear nonlocal electron−phonon coupling constants.

In order to quantify the strength of the nonlocal electron−phonon coupling and characterize the global impact of *all* crystal vibrations, it is useful to take advantage of the parameters $G$ and $L$ that have been introduced in our previous work:[19]

$$G_{mn}^2 = \sum_j \frac{v_{jmn}^2}{2} \tag{4}$$

$$L_{mn} = \sum_j \frac{v_{jmn}^2}{2\hbar\omega_j} \tag{5}$$

There are two main aspects that are important to highlight regarding $G$ and $L$. First, it was shown[19] that $L$ can be viewed as playing, in the context of *nonlocal* electron−vibration coupling, a role similar to that played by the reorganization energy (polaron binding energy)[16,17,19] in the case of the *local* vibrational coupling mechanism. Second, $G$ and $L$ are also directly related to the variance (and, thus, to the modulation) of the transfer integrals due to thermal fluctuations:

$$\sigma^2 = \langle (t_{mn} - \langle t_{mn}\rangle)^2\rangle = \langle t_{mn}^2\rangle - \langle t_{mn}\rangle^2 \tag{6}$$

$$\langle t_{mn}\rangle = t_{mn}^{(0)} \tag{7}$$

$$\sigma^2 = \sum_j \frac{v_{jmn}^2}{2} \coth\left(\frac{\hbar\omega_j}{2k_B T}\right) \tag{8}$$

Here, the notation $\langle A\rangle$ represents the thermal average of any given operator $A$ over the lattice phonons:[32]

$$\langle A\rangle = \mathrm{Tr}[\exp(-H_L/k_B T)A]/\mathrm{Tr}[\exp(-H_L/k_B T)] \tag{9}$$

where $H_L$ is the lattice Hamiltonian given by eq 2. In the limiting cases of low ($\hbar\omega \gg k_B T$) and high ($\hbar\omega \ll k_B T$) temperatures, eq 8 reduces to[19]

$$\sigma^2 = \begin{cases} G^2; & \hbar\omega \gg k_B T \\ 2Lk_B T; & \hbar\omega \ll k_B T \end{cases} \tag{10}$$


(18) Peierls, R. E. *Quantum theory of solids*; Clarendon Press: Oxford, 1955.
(19) Coropceanu, V.; Sánchez-Carrera, R. S.; Paramonov, P.; Day, G. M.; Brédas, J.-L. *J. Phys. Chem. C* **2009**, *113*, 4679.
(20) Della Valle, R. G.; Brillante, A.; Farina, L.; Venuti, E.; Masino, M.; Girlando, A. *Mol. Cryst. Liq. Cryst.* **2004**, *416*, 145.
(21) Fratini, S.; Ciuchi, S. *Phys. Rev. Lett.* **2009**, *103*, 266601.
(22) Hannewald, K.; Bobbert, P. A. *Appl. Phys. Lett.* **2004**, *85*, 1535.
(23) Kwiatkowski, J. J.; Frost, J. M.; Kirkpatrick, J.; Nelson, J. *J. Phys. Chem. A* **2008**, *112*, 9113.
(24) Martinelli, N. G.; Olivier, Y.; Athanasopoulos, S.; Ruiz-Delgado, M. C.; Pigg, K. R.; da Silva, D. A.; Sánchez-Carrera, R. S.; Venuti, E.; Della Valle, R. G.; Brédas, J. L.; Beljonne, D.; Cornil, J. *ChemPhysChem* **2009**, *10*, 2265.
(25) Masino, M.; Girlando, A.; Brillante, A.; Farina, L.; Della Valle, R. G.; Venuti, E. *Macromol. Symp.* **2004**, *212*, 375.
(26) Sun, J.; Zhao, Y.; Liang, W. Z. *Phys. Rev. B* **2009**, *79*, 155112.
(27) Troisi, A.; Cheung, D. L.; Andrienko, D. *Phys. Rev. Lett.* **2009**, *102*, 116602.
(28) Troisi, A.; Orlandi, G. *J. Phys. Chem. A* **2006**, *110*, 4065.
(29) Troisi, A.; Orlandi, G. *Phys. Rev. Lett.* **2006**, *96*, 086601.
(30) Wang, L. J.; Peng, Q.; Li, Q. K.; Shuai, Z. *J. Chem. Phys.* **2007**, *127*, 044506.
(31) Zhao, Y.; Li, G. Q.; Sun, J.; Wang, W. H. *J. Chem. Phys.* **2008**, *129*, 124114.
(32) Kubo, R. *Statistical mechanics, an advanced course with problems and solutions*; North-Holland Pub. Co.: Amsterdam, 1965.

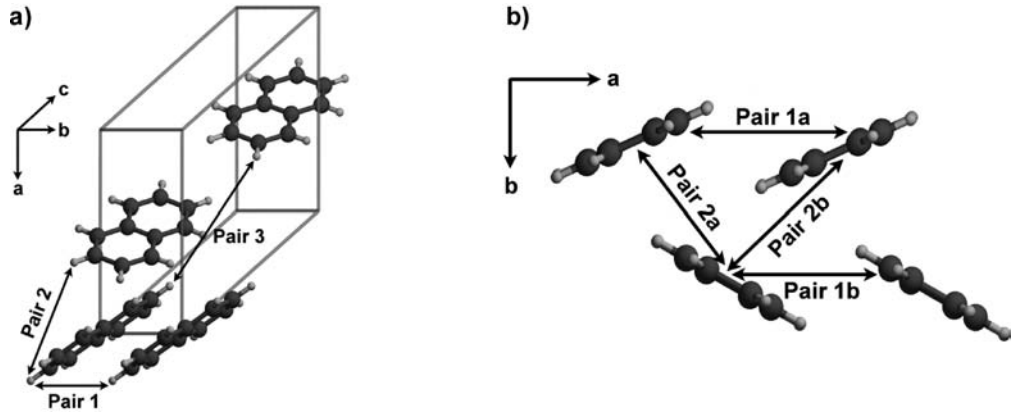


***Figure 1.*** (a) Illustration of the crystal structure of naphthalene and of the molecular pairs with the largest transfer integrals considered in the calculations (molecular pairs are defined in the same way in anthracene). (b) Definition of the molecular dimers used to compute the transfer integrals in the tetracene and pentacene crystals (here, viewed down the *c*-axis).

***Table 1.*** Crystallographic Parameters at Experimental Temperatures and MM-Optimized Unit-Cell Parameters for Oligoacenes

| structure | *T* (K) | *a* (Å) | *b* (Å) | *c* (Å) | α (deg) | *β* (deg) | *γ* (deg) |
|---|---|---|---|---|---|---|---|
| naphthalene[43] (monoclinic) | 123 | 8.098 | 5.953 | 8.652 | 90.0 | 124.4 | 90.0 |
| anthracene[44] (monoclinic) | 94 | 8.4144 | 5.9903 | 11.0953 | 90.0 | 125.293 | 90.0 |
| tetracene[45] (triclinic) | 175 | 6.0565 | 7.8376 | 13.0104 | 77.127 | 72.118 | 85.792 |
| pentacene[45] (triclinic) | 180 | 6.2753 | 7.7138 | 14.4424 | 76.752 | 88.011 | 84.524 |
| | | | MM-Optimized Parameters | | | | |
| naphthalene (monoclinic) | | 8.1457 | 6.0329 | 8.7163 | 90.0 | 122.471 | 90.0 |
| anthracene (monoclinic) | | 8.3611 | 6.1161 | 11.1668 | 90.0 | 123.532 | 90.0 |
| tetracene (triclinic) | | 6.2311 | 7.6318 | 13.5667 | 76.699 | 70.226 | 86.369 |
| pentacene (triclinic) | | 6.3195 | 7.6260 | 15.0194 | 78.413 | 83.859 | 85.930 |

The geometric structure and electronic properties of the oligoacene crystals were computed at the density functional theory (DFT) level, using the Perdew−Burke−Ernzerhof exchange-correlation functional with a plane-wave basis set (300 eV cutoff) and projector augmented wave potentials.[33,34] DFT geometry optimizations were performed by constraining the cell parameters to the experimental values (see Table 1). The self-consistent calculations were carried out with an $8\times8\times8$ *k*-point mesh. The Γ-point lattice phonons were derived by means of numerical differentiation using a 0.03 Å atomic displacement step. All DFT crystal structure calculations were carried out using the VASP code.[35]

The crystal structures and the lattice dynamics at the Γ-point were also investigated by means of molecular mechanics (MM) simulations using the DMAREL program.[36] An empirical Buckingham (exp-6) model[37] was used for the repulsion−dispersion interactions, and the atomic point charges were determined from MP2/6-31G** (naphthalene and anthracene) and DFT B3LYP/6-31G** (tetracene and pentacene) calculations, using the CHelpG algorithm as implemented in the Gaussian03 package.[38] The MM lattice energy minimization and lattice dynamics calculations were carried out in the framework of the rigid-molecule approximation.[39,40] The molecular geometries were fixed at those found in the experimentally determined crystal structures, with C−H bond lengths normalized to 1.08 Å. Electrostatic interactions were evaluated using Ewald summations; all other interactions were summed to a 15 Å cutoff (Tables S1−S5 in the Supporting Information provide a complete list of the molecular geometries and force-field parameters used in the MM simulations). The unit-cell dimensions were allowed to relax during the MM geometry optimizations, and the root-mean-square (rms) percentage changes in unit-cell lengths were 0.9% in naphthalene, 1.3% in anthracene, 3.3% in tetracene, and 2.4% in pentacene; the optimized unit-cell parameters are reported in Table 1. Second derivatives of the lattice energy with respect to molecular translations and rotations about molecular inertial axes were obtained by numerical differentiation.

The transfer integrals between selected nearest-neighbor pairs of molecules were evaluated at both DFT-optimized and MM-optimized crystal geometries by using a fragment orbital approach in combination with a basis set orthogonalization procedure.[41] All transfer integrals were evaluated at the DFT level with the PW91 functional and Slater-type triple-ζ plus polarization basis sets for all atoms using the ADF package.[42]

## 3. Results and Discussion

**Crystallographic Information.** The crystal structures of naphthalene[43] and anthracene[44] are monoclinic with the space group $P2_1/a$, while tetracene[45] and pentacene[45] crystallize in the triclinic $P\bar{1}$ space group; the experimental cell parameters are given in Table 1. The arrangement of the molecules within the unit cell of these crystals is very similar (see Figure 1). In all

(33) Blochl, P. E. *Phys. Rev. B* **1994**, *50*, 17953.
(34) Kresse, G.; Joubert, D. *Phys. Rev. B* **1999**, *59*, 1758.
(35) Kresse, G.; Furthmuller, J. *Comput. Mater. Sci.* **1996**, *6*, 15.
(36) Willock, D. J.; Price, S. L.; Leslie, M.; Catlow, C. R. A. *J. Comput. Chem.* **1995**, *16*, 628.
(37) Williams, D. E.; Cox, S. R. *Acta Crystallogr., Sect. B: Struct. Sci.* **1984**, *40*, 404.
(38) Frisch, M. J., et al. *Gaussian03*; Gaussian, Inc: Wallingford, CT, 2004.
(39) Brüesch, P. *Phonons, theory and experiments*; Springer-Verlag: Berlin, 1982.
(40) Day, G. M.; Price, S. L.; Leslie, M. *J. Phys. Chem. B* **2003**, *107*, 10919.
(41) Valeev, E. F.; Coropceanu, V.; da Silva Filho, D. A.; Salman, S.; Brédas, J. L. *J. Am. Chem. Soc.* **2006**, *128*, 9882.
(42) Velde, G. T.; Bickelhaupt, F. M.; Baerends, E. J.; Guerra, C. F.; Van Gisbergen, S. J. A.; Snijders, J. G.; Ziegler, T. *J. Comput. Chem.* **2001**, *22*, 931.
(43) Ponomarev, V. I.; Filipenko, O. S.; Atovmyan, L. O. *Kristallografiya* **1976**, *21*, 392.
(44) Brock, C. P.; Dunitz, J. D. *Acta Crystallogr., Sect. B: Struct. Sci.* **1990**, *46*, 795.
(45) Holmes, D.; Kumaraswamy, S.; Matzger, A. J.; Vollhardt, K. P. C. *Chem.−Eur. J.* **1999**, *5*, 3399.

***Table 2.*** DFT Estimates of the Transfer Integrals (in meV) in the Naphthalene and Anthracene Crystals Using the DFT- and MM-Optimized Crystal Geometries

| | naphthalene | | | | anthracene | | | |
|---|---|---|---|---|---|---|---|---|
| | MM geometry | | DFT geometry | | MM geometry | | DFT geometry | |
| | hole | electron | hole | electron | hole | electron | hole | electron |
| pair 1 | −31.1 | 16.7 | −35.6 | 14.1 | −38.8 | 25.8 | −44.9 | 36.9 |
| pair 2 | −19.6 | −26.7 | −12.0 | −35.3 | 14.5 | −52.2 | −18.6 | 61.6 |
| pair 3 | 13.0 | −6.3 | 17.9 | −5.7 | −15.0 | 2.4 | 18.6 | −2.6 |

***Table 3.*** DFT Estimates of the Transfer Integrals (in meV) in the Tetracene and Pentacene Crystals Using the DFT- and MM-Optimized Crystal Geometries

| | tetracene | | | | pentacene | | | |
|---|---|---|---|---|---|---|---|---|
| | MM geometry | | DFT geometry | | MM geometry | | DFT geometry | |
| | hole | electron | hole | electron | hole | electron | hole | electron |
| pair 1a | −13.0 | −1.8 | −5.1 | −12.6 | 1.4 | −26.1 | 33.8 | −43.1 |
| pair 1b | 1.0 | −27.6 | 13.2 | −32.8 | 3.3 | −29.3 | 35.7 | −44.8 |
| pair 2a | −2.3 | 63.8 | 17.1 | 63.9 | 11.1 | 89.2 | 47.3 | −82.5 |
| pair 2b | −76.9 | −75.8 | −69.5 | −67.3 | −73.3 | −80.4 | −85.2 | 83.5 |

***Table 4.*** Intermolecular Center-to-Center Distances (in Å) for the Dimers within the *ab*-Plane of Oligoacenes, Derived from the DFT-Optimized Crystal Geometries

| | pair 1a (1b) | pair 2a | pair 2b |
|---|---|---|---|
| naphthalene | 5.95 | 5.03 | 5.03 |
| anthracene | 5.99 | 5.16 | 5.16 |
| tetracene | 6.06 | 5.13 | 4.77 |
| pentacene | 6.28 | 5.20 | 4.73 |

instances, there exist two molecules per unit cell ($Z = 2$), and all molecules occupy crystallographic inversion centers at (0,0,0) and ($^1/_2$,$^1/_2$,0). In the case of the naphthalene and anthracene crystals, these two molecules are symmetrically equivalent, while the two molecules in the unit cell are symmetrically independent in the tetracene and pentacene crystals.

**Transfer Integrals.** As described elsewhere,[46,47] in the naphthalene and anthracene crystals, significant electronic couplings are found not only along the short crystal axis (pair 1 in Figure 1a) but also along the diagonal directions of the unit cell (pair 2 and pair 3); the calculated transfer integrals for the three most relevant dimers are given in Table 2. In the case of tetracene and pentacene, the electronic couplings along the *c*-axis are vanishingly small. Therefore, the discussion for these systems will be limited to the interactions within the *ab* plane (see Figure 1b); the calculated transfer integrals for tetracene and pentacene are given in Table 3.

While transfer integrals generally decay exponentially with intermolecular distances (see Table 4 for a list of such distances related to the pairs of molecules considered here), in accordance with previous studies,[46] it is found that intermolecular *orientations* can also substantially impact the electronic couplings. For instance, pair 2a in tetracene and pentacene has an intermolecular distance about 0.4−0.5 Å larger than that in pair 2b; however, the transfer integrals for electrons in these two pairs are essentially the same. The data in Tables 2 and 3 also show that the transfer integrals of the herringbone dimers are larger for systems with larger molecules; no obvious trend is found for the cofacial dimers.

***Table 5.*** Phonon Frequencies of the Intermolecular Optical Modes in the Naphthalene ($C_{10}H_8$) and Anthracene ($C_{14}H_{10}$) Crystals Obtained from MM and DFT Normal-Mode Calculations[a]

| type | MM | DFT | expt[b] |
|---|---|---|---|
| | Naphthalene | | |
| translation | 50 | 51 | 44 |
| libration | 54 | 56 | 56 |
| libration | 59 | 63 | 67 |
| translation | 63 | 76 | 75 |
| libration | 82 | 97 | 83 |
| libration | 99 | 102 | 88 |
| translation | 117 | 121 | 106 |
| libration | 152 | 126 | 121 |
| libration | 153 | 150 | 141 |
| | Anthracene | | |
| translation | 43 | 44 | 47 |
| libration | 47 | 46 | 48 |
| libration | 55 | 54 | 54 |
| translation | 59 | 73 | 69 |
| libration | 78 | 90 | 70 |
| libration | 91 | 97 | 77 |
| translation | 120 | 120 | 106 |
| libration | 158 | 133 | 122 |
| libration | 161 | 149 | 130 |

[a] All values are in $cm^{-1}$. [b] The experimental frequencies for naphthalene (observed at 15 K) and anthracene (observed at 12 K) were taken from refs 50 and 51, respectively.

**Γ-Point Lattice Phonons.** The lattice dynamical properties of the oligoacene crystals have been computed at the Γ-point of the Brillouin zone. In the rigid-body approximation,[48] the presence of two molecules in the unit cell results in 12 intermolecular vibration modes. Among these modes, three are acoustic and the other nine are optical. In the more general case where intramolecular motions are also taken into account, there occur $9 + 2n_i$ optical modes, where $n_i$ denotes the number of intramolecular degrees of freedom and the factor of 2 is related to the presence of two molecules per unit cell. The phonon frequencies of the lowest nine optical modes from MM and DFT calculations are collected in Tables 5 and 6.

The MM and DFT estimates are generally in good mutual agreement and also compare very well with the available experimental data. However, some discrepancies between these two approaches are evident. One or both of the highest-energy librational modes are overestimated in the MM calculations in comparison to both DFT and the experimental measurements. (While it is tempting to associate the overestimation in these frequencies to the rigid-body approximation, Filippini and Gramaccioli's earlier study[49] on tetracene and pentacene demonstrated that coupling of these lattice modes to intramolecular vibrations only results in shifts of a few wavenumbers; in fact, it appears that the errors in these highest-frequency librational modes are rather related to the choice of the repulsion−dispersion exp-6 parameters; the highest-frequency librational modes in naphthalene have been shown indeed to be particularly sensitive to the repulsion-dispersion model.[40])

(46) Brédas, J. L.; Calbert, J. P.; da Silva Filho, D. A.; Cornil, J. *Proc. Natl. Acad. Sci. U.S.A.* **2002**, *99*, 5804.
(47) Cheng, Y. C.; Silbey, R. J.; da Silva Filho, D. A.; Calbert, J. P.; Cornil, J.; Brédas, J. L. *J. Chem. Phys.* **2003**, *118*, 3764.
(48) Califano, S.; Schettino, V.; Neto, N. *Lattice dynamics of molecular crystals*; Springer-Verlag: Berlin, 1981.
(49) Filippini, G.; Gramaccioli, C. M. *Chem. Phys. Lett.* **1984**, *104*, 50.
(50) Suzuki, M.; Yokoyama, T.; Ito, M. *Spectrochim. Acta, Part A* **1968**, *24*, 1091.
(51) Dorner, B.; Bokhenkov, E. L.; Chaplot, S. L.; Kalus, J.; Natkaniec, I.; Pawley, G. S.; Schmelzer, U.; Sheka, E. F. *J. Phys. C: Solid State Phys.* **1982**, *15*, 2353.

***Table 6.*** Phonon Frequencies of the Intermolecular Optical Modes in the Tetracene ($C_{18}H_{12}$) and Pentacene ($C_{22}H_{14}$) Crystals Obtained from MM and DFT Normal-Mode Calculations[a]

| type | MM | DFT | expt[b] |
|---|---|---|---|
| | Tetracene | | |
| translation | 30 | 37 | |
| libration | 46 | 48 | 44−45 |
| libration | 50 | 52 | 49 |
| translation | 55 | 72 | |
| libration | 73 | 81 | 61 |
| libration | 102 | 110 | 94 |
| translation | 120 | 119 | |
| libration | 153 | 132 | 120 |
| libration | 161 | 146 | 132 |
| | Pentacene | | |
| translation | 20 | 45 | |
| libration | 35 | 48 | 45 |
| libration | 57 | 63 | 66 |
| translation | 53 | 74 | |
| libration | 68 | 85 | 84 |
| libration | 102 | 112 | 99 |
| translation | 123 | 125 | |
| libration | 156 | 139 | 144 |
| libration | 162 | 153 | 150 |

[a] All values are in $cm^{-1}$. [b] The experimental frequencies (where available) for tetracene (observed at 296 K) and pentacene (observed at 79 K) were taken from ref 52 and refs 53 and 54, respectively.

The MM and DFT calculations also differ for all four oligoacene crystals in their description of the lowest-energy translational vibrational mode that, as shown below, interacts strongly with both electrons and holes. (In contrast to the DFT calculations, the MM values for the frequency of this mode decrease sharply as the size of the molecule increases. While the agreement for this mode between MM and DFT is rather good in the case of naphthalene and anthracene, the MM value in pentacene is about twice as small as the DFT value.) The lack of experimentally determined frequencies for this mode prevents a definitive assessment of which method performs more reliably. However, since DFT reproduces most of the observed pentacene frequencies better than MM, it is likely that the MM calculations actually underestimate the energy of this mode.

As the molecules in the oligoacene structures lie on crystallographic inversion centers, the translational and librational motions do not mix; as a result, the nine intermolecular modes can be classified into three pure translational modes and six pure librational modes. In addition, the symmetry of the monoclinic $P2_1/a$ space group implies that the two molecules in the unit cell are related by symmetry transformations. Therefore, in the naphthalene and anthracene crystals, the translationally nonequivalent molecules in each mode move in-phase or out-of-phase along similar molecular axes. There are no such symmetry restrictions in the case of the tetracene and pentacene crystals; thus, the translationally nonequivalent molecules can move along different molecular axes (see Figure S2 in the Supporting Information).

Since the DFT calculations are not based on the rigid-body approximation, they reveal that some mixing can occur between the intermolecular and intramolecular vibrations and that this mixing is more pronounced in larger systems. This feature can be explained by the fact that the energy of lower-frequency intramolecular vibrations becomes smaller in larger molecules, which results in a closer energetic overlap between intra- and intermolecular vibrations.

(52) Jankowiak, R.; Kalinowski, J.; Konys, M.; Buchert, J. *Chem. Phys. Lett.* **1979**, *65*, 549.
(53) Tomkiewicz, Y.; Groff, R. P.; Avakian, P. *J. Chem. Phys.* **1971**, *54*, 4504.
(54) Della Valle, R. G.; Venuti, E.; Farina, L.; Brillante, A.; Masino, M.; Girlando, A. *J. Phys. Chem. B* **2004**, *108*, 1822.

***Table 7.*** DFT Estimates of $t^{(0)}$, $L$, and $G$ in the Naphthalene and Anthracene Crystals Based on the MM-Optimized Geometries and Normal Modes[a]

| | holes | | | electrons | | |
|---|---|---|---|---|---|---|
| | pair 1 | pair 2 | pair 3 | pair 1 | pair 2 | pair 3 |
| | | | Naphthalene | | | |
| $t^{(0)}$ | −31.1 | −19.6 | 13.0 | 16.7 | −26.7 | −6.3 |
| $L$ | 11.3 | 15.8 | 1.1 | 38.8 | 30.6 | 1.8 |
| $G$ | 10.0 | 11.0 | 2.7 | 17.0 | 15.8 | 4.0 |
| | | | Anthracene | | | |
| $t^{(0)}$ | −38.8 | 14.5 | −15.0 | 25.8 | −52.2 | 2.4 |
| $L$ | 4.4 | 13.8 | 0.9 | 12.8 | 13.0 | 0.9 |
| $G$ | 5.7 | 10.4 | 2.4 | 9.0 | 10.4 | 2.6 |

[a] All parameters are given in meV.

***Table 8.*** DFT Estimates of $t^{(0)}$, $L$, and $G$ in the Tetracene and Pentacene Crystals Based on the MM-Optimized Geometries and Normal Modes[a]

| | holes | | | | electrons | | | |
|---|---|---|---|---|---|---|---|---|
| | pair 1a | pair 1b | pair 2a | pair 2b | pair 1a | pair 1b | pair 2a | pair 2b |
| | | | | Tetracene | | | | |
| $t^{(0)}$ | −13.0 | 1.0 | −2.3 | −76.9 | −1.8 | −27.6 | 63.8 | −75.8 |
| $L$ | 2.7 | 3.3 | 11.5 | 8.7 | 3.9 | 3.4 | 9.6 | 3.1 |
| $G$ | 4.1 | 4.7 | 7.2 | 10.8 | 4.9 | 4.6 | 7.9 | 5.9 |
| | | | | Pentacene | | | | |
| $t^{(0)}$ | 1.4 | 3.3 | 11.1 | −73.3 | −26.1 | −29.3 | 89.2 | −80.4 |
| $L$ | 0.8 | 1.3 | 17.1 | 12.1 | 0.7 | 1.0 | 3.2 | 2.1 |
| $G$ | 2.6 | 2.9 | 7.7 | 10.1 | 2.2 | 2.4 | 6.2 | 5.4 |

[a] All parameters are given in meV.

**Nonlocal Electron−Phonon Couplings.** The linear nonlocal electron−phonon coupling constants (see eq 3), $\upsilon_{jmn} = \partial t_{mn}/\partial Q_j$, are computed numerically. This is achieved by first distorting the crystal along all normal-mode coordinates and then computing the related transfer integrals for each distorted geometry; in the following step, the derivatives of the transfer integrals with respect to normal coordinates are evaluated. The electron− and hole−phonon coupling constants derived from the MM normal-mode calculations are given in the Supporting Information (Tables S6−S9); the $L$ and $G$ parameters along with the corresponding transfer integrals are collected in Tables 7 and 8.

In an optical translation-type mode at the Γ-point, all translationally equivalent molecules move in-phase; therefore, such translational modes do not contribute to the nonlocal coupling related to cofacial dimers (pair 1 in naphthalene and anthracene; pairs 1a and 1b in tetracene and pentacene). In contrast, in the case of dimers containing translationally nonequivalent molecules, the translational modes contribute to the nonlocal interactions in addition to the librational modes.

The $L$ and $G$ parameters derived from the DFT normal-mode calculations are given in Tables 9 and 10 (all electron−phonon couplings are collected in Tables S10−S13 in the Supporting Information). While the results obtained using the normal modes from DFT calculations or MM simulations provide comparable trends, it is important to recall that the DFT calculations go beyond the rigid-body approximation and therefore allow an evaluation of the nonlocal couplings due to intramolecular vibrations. The results are given in Tables S10−S13 for the four crystals and illustrated in Figure 2 for the anthracene crystal.

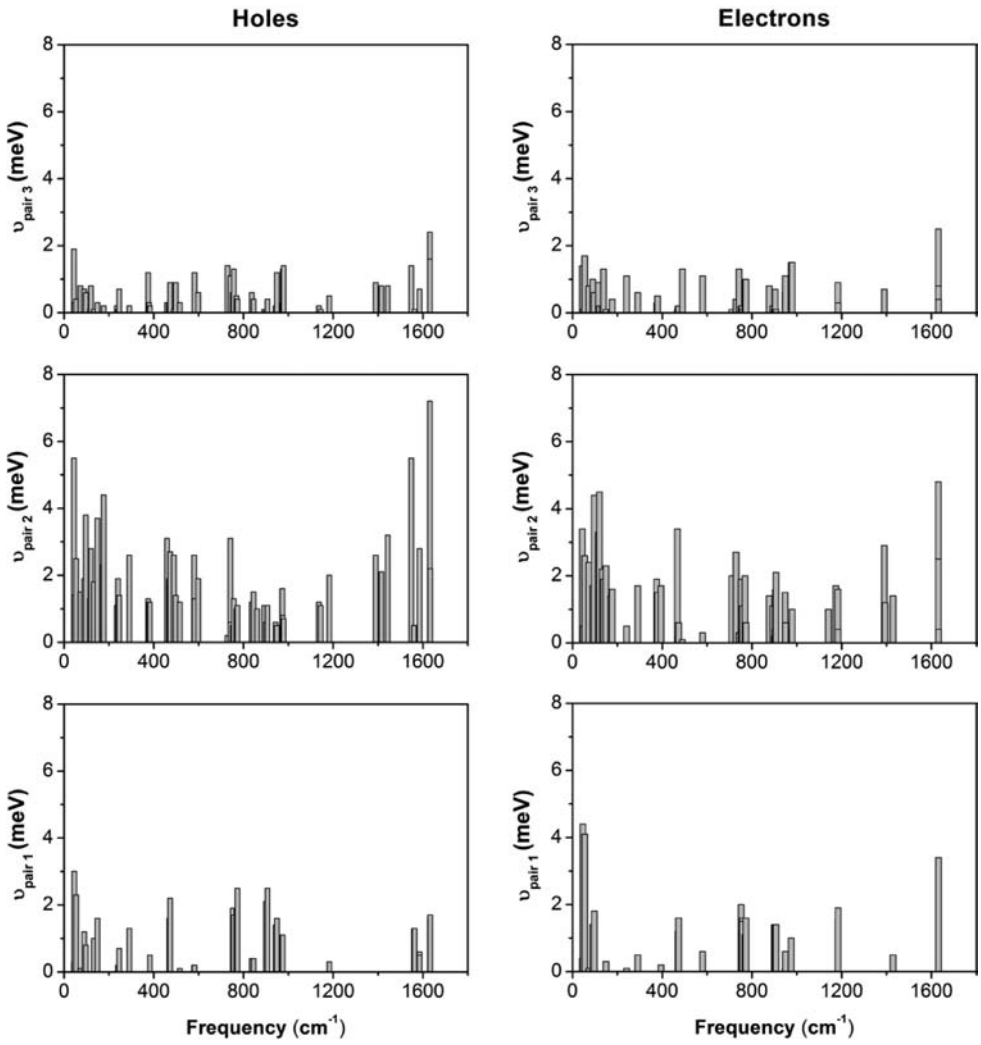


***Figure 2.*** DFT estimates of the hole−phonon and electron−phonon couplings in the anthracene crystal as a function of phonon energy.

***Table 9.*** DFT Estimates of $t^{(0)}$, $L$, and $G$ in the Naphthalene and Anthracene Crystals Based on the DFT-Optimized Geometries and Normal Modes[a]

| | holes | | | electrons | | |
|---|---|---|---|---|---|---|
| | pair 1 | pair 2 | pair 3 | pair 1 | pair 2 | pair 3 |
| | | | Naphthalene | | | |
| $t^{(0)}$ | −35.6 | −12.0 | 17.9 | 14.1 | −35.3 | −5.7 |
| $L$ | 3.6 | 7.3 | 0.8 | 12.9 | 10.0 | 1.1 |
| $G$ | 9.3 | 16.0 | 5.8 | 15.2 | 15.6 | 6.0 |
| | | | Anthracene | | | |
| $t^{(0)}$ | −44.9 | −18.6 | 18.6 | 36.9 | 61.6 | −2.6 |
| $L$ | 1.7 | 6.9 | 0.7 | 3.5 | 5.0 | 0.7 |
| $G$ | 6.3 | 13.1 | 4.8 | 7.3 | 10.4 | 4.5 |

[a] All parameters are given in meV.

***Table 10.*** DFT Estimates of $t^{(0)}$, $L$, and $G$ in the Tetracene and Pentacene Crystals Based on the DFT-Optimized Geometries and Normal Modes[a]

| | holes | | | | electrons | | | |
|---|---|---|---|---|---|---|---|---|
| | pair 1a | pair 1b | pair 2a | pair 2b | pair 1a | pair 1b | pair 2a | pair 2b |
| | | | | Tetracene | | | | |
| $t^{(0)}$ | −5.1 | 13.2 | 17.1 | −69.5 | −12.6 | −32.8 | 63.9 | −67.3 |
| $L$ | 2.9 | 4.0 | 5.6 | 5.4 | 3.9 | 4.5 | 4.7 | 4.5 |
| $G$ | 6.4 | 7.5 | 10.7 | 10.8 | 6.7 | 7.0 | 9.0 | 8.6 |
| | | | | Pentacene | | | | |
| $t^{(0)}$ | 33.8 | 35.7 | 47.3 | −85.2 | −43.1 | −44.8 | −82.5 | 83.5 |
| $L$ | 1.5 | 1.5 | 5.0 | 4.8 | 1.0 | 1.0 | 2.7 | 3.0 |
| $G$ | 5.7 | 5.7 | 10.7 | 10.5 | 4.5 | 4.5 | 8.1 | 8.2 |

[a] All parameters are given in meV.

In agreement with our previous results,[19] the results point to a significant contribution of the intramolecular vibrations to the values of $L$ and $G$; in fact, in many instances, the largest couplings calculated at the DFT level are found for high-frequency modes. In the case of naphthalene, we have shown[19] that the coupling with high-frequency modes is due to the fact that distortions along such modes can significantly affect the electron-density distribution of the frontier molecular orbitals; this, as a consequence, has a major effect on the intermolecular overlap integrals. Interestingly, this effect appears to be general and not limited to the naphthalene crystal.

Previous investigations[9,55,56] have shown that the reorganization energy $\lambda$ related to the local (Marcus−Holstein type) coupling exhibits a molecular-size dependence going as $1/N$, where $N$ is the number of $\pi$-electrons. The calculations based

(55) Coropceanu, V.; Malagoli, M.; da Silva Filho, D. A.; Gruhn, N. E.; Bill, T. G.; Brédas, J. L. *Phys. Rev. Lett.* **2002**, *89*, 275503.
(56) Devos, A.; Lannoo, M. *Phys. Rev. B* **1998**, *58*, 8236.

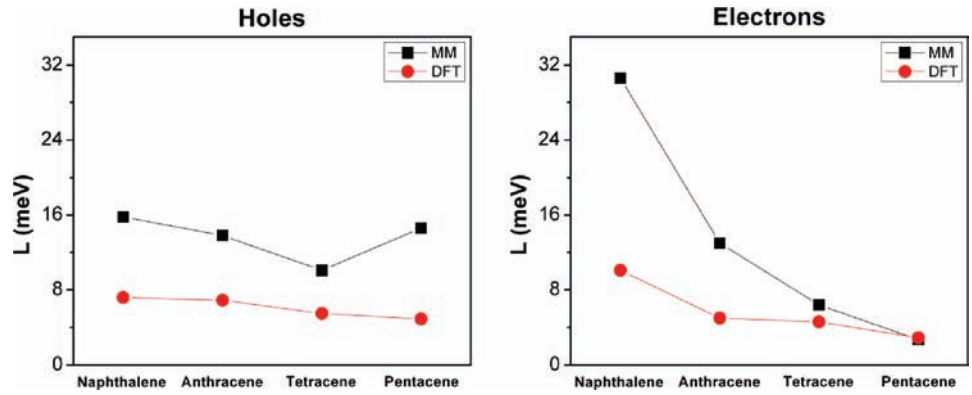


***Figure 3.*** Estimates of $L$ based on MM and DFT normal-mode results for herringbone dimers (in tetracene and pentacene, $L$ is averaged over pairs 2a and 2b).

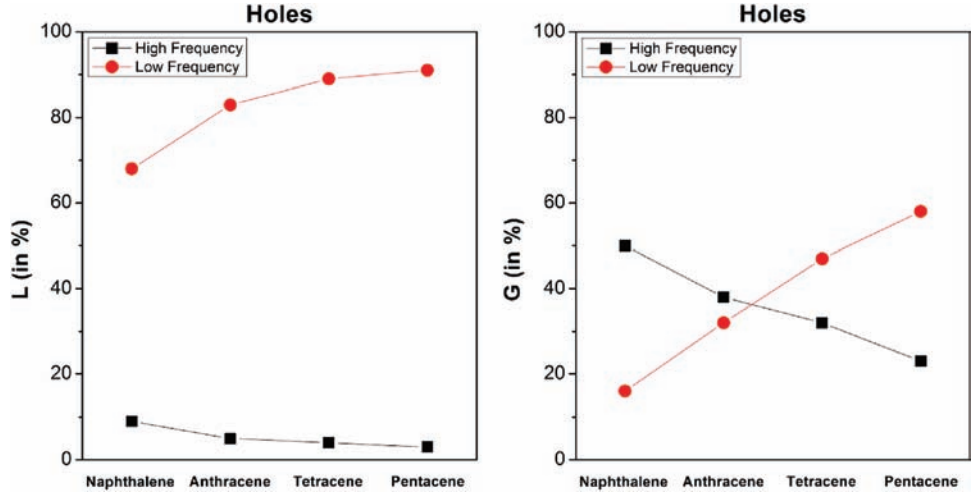


***Figure 4.*** DFT normal-mode-based contributions (in percentage) of low-energy vibrations (<200 $cm^{-1}$) and high-energy vibrations (>1000 $cm^{-1}$) to $L$ and $G$ for herringbone-type dimers (in tetracene and pentacene, $L$ and $G$ are averaged over pairs 2a and 2b).

on the DFT normal modes indicate (see Figure 3) that the relaxation energy $L$ associated with the nonlocal electron−phonon coupling *also decreases* as the size of the molecule increases, although in a manner less straightforward than that of $\lambda$. This size dependence is more pronounced for electrons than for holes, which is also the case for $\lambda$ in oligoacenes.[55] Note that the calculations based on the MM normal modes show similar trends, with the exception of the results obtained for holes in pentacene. The $L$ value for holes in pentacene is possibly overestimated due to the underestimation of the frequency of the lowest vibration mode by MM calculations, *vide supra*.

It is worth stressing that these trends are somewhat unexpected. Indeed, the nonlocal coupling constants correspond to first-order derivatives of the electronic couplings; thus, it would be reasonable to expect that the larger the transfer integrals, the larger the impact of vibrations, and the larger the nonlocal coupling constants. However, inspection of Tables 7−10 does not reveal any clear relationship between the transfer integrals and the electron−phonon couplings constants. It is interesting to recall that, in our previous work,[19] it was shown that $L$ represents the relaxation energy of the delocalized [resonance] states of a charged dimer when the dependence of the transfer integral [resonance interaction] on the vibration coordinates is taken into account. In the context of potential energy surfaces, it then appears logical that the relaxation energy $L$ decreases as the system size increases. At this stage, it remains, however, premature to assess whether the inverse relationship found between $L$ and molecular size is a general feature and reflects an intrinsic physical property of organic semiconductors or whether it is specific to the present class of systems.

We have also computed the relative contributions to $L$ and $G$ coming from the lowest-frequency vibrations (frequencies < 200 $cm^{-1}$), which are mainly *inter*molecular, and from the highest-frequency vibrations (frequencies > 1000 $cm^{-1}$), which are mainly *intra*molecular. The results obtained for holes are plotted in Figure 4. They highlight that the relative contribution from the lowest-frequency phonons to $L$ and $G$ increases as a function of molecular size, while the relative contribution from the highest-frequency phonons decreases. The same dependence of $L$ and $G$ on phonon energies is found for electrons (see Supporting Information).

**Thermal Fluctuations.** Assuming either classical or quantum-mechanical statistics, we have calculated the standard deviations of the transfer integrals ($\sigma_{Cl}$ and $\sigma_{QM}$) on the basis of the DFT normal modes. The results are shown in Figures 5 and 6.

The values of $\sigma_{QM}$ at 0 K in the naphthalene and anthracene crystals are found to be about 60−70% of those at room temperature (Figure 5). The $\sigma_{QM}$ and $\sigma_{Cl}$ values in these systems differ substantially even at high temperatures (for instance, by up to 15% in the case of holes in naphthalene at room temperature); this implies that, for naphthalene and anthracene, the vibrations should be treated at the quantum-mechanical level, even at elevated temperatures. The zero-point fluctuations have a smaller contribution in the case of the tetracene and pentacene

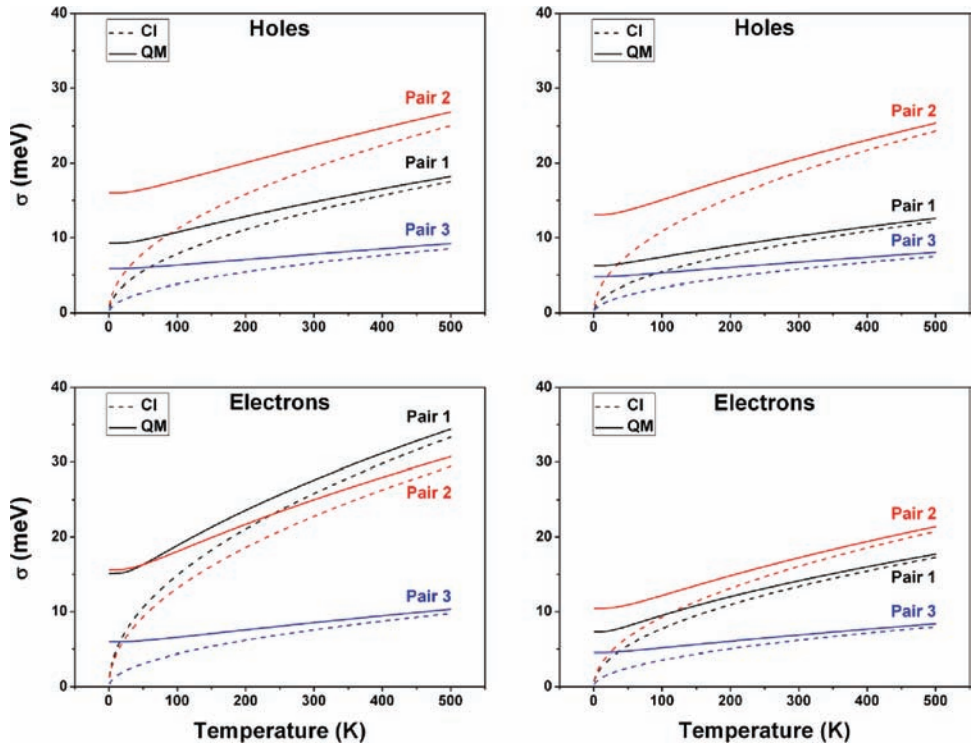


***Figure 5.*** Classical and quantum-mechanical standard deviations for the transfer integrals in the naphthalene (left) and anthracene (right) crystals derived on the basis of DFT normal-mode calculations.

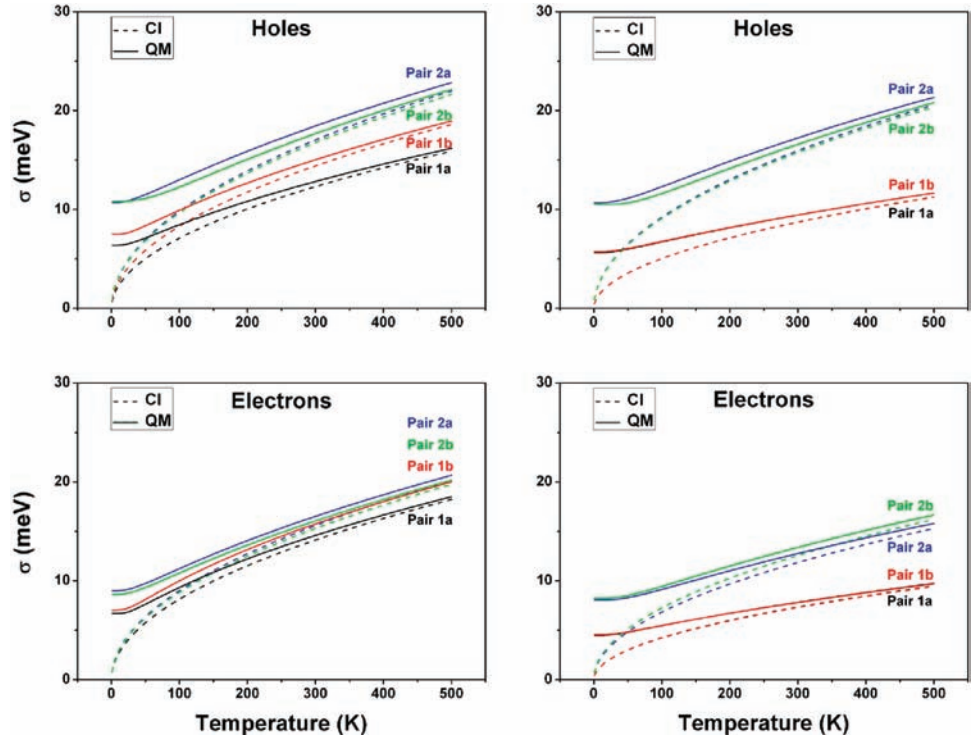


***Figure 6.*** Classical and quantum-mechanical standard deviations for the transfer integrals in the tetracene (left) and pentacene (right) crystals derived on the basis of DFT normal-mode calculations.

crystals; the $\sigma_{QM}$ values at 0 K for both holes and electrons are in these instances about 40% of the value found at room temperature (Figure 6). Around room temperature, $\sigma_{QM}$ and $\sigma_{Cl}$ are in general close to each other. This is a consequence of the observed increase in the contribution from low-frequency vibrations to the nonlocal coupling as the size of the system is increasing. Thus, our results suggest that, around room temperature, semiclassical approaches could be more apt to model charge transport in the larger oligoacenes in comparison to the smaller systems.

**Phonon-Assisted Charge Transport.** Microscopic charge-transport models based on a Holstein−Peierls-type Hamiltonian

were worked out initially by Munn and Silbey[14,15] and later by Bobbert and co-workers.[12,22] More recently, Troisi and Orlandi[29] as well as Fratini and Ciuchi[21] have discussed the problem of charge transport in organic semiconductors by means of semiclassical approaches (treating the vibrations classically). In spite of the major approximations that had to be made in these theoretical models, they all suggest that there can exist qualitatively different transport scenarios as a function of the values of the microscopic parameters and the temperature.

The effects of vibrations on charge transport include two main factors: (i) scattering processes due to phonons and (ii) phonon-assisted transport. The general picture is somewhat simpler to grasp in the framework of semiclassical models. At this level of theory,[21] the effect of nonlocal coupling on the transport properties is described by the parameter $L$. Since the formulation of a comprehensive charge-transport theory remains challenging, we restrict our discussion to the two limiting transport regimes, namely, the band-like regime and the hopping regime. (We recall that both mechanisms can be operative in the same system, with the former dominant at low temperatures and the latter at high temperatures.) According to band theory, a charge moves coherently in a wave-like manner and is scattered (or relaxed) by phonons from one momentum state to another. The carrier mobility in wide electronic bands is given by

$$\mu = \frac{q\tau}{m} \tag{11}$$

where $q$ denotes the charge of the carrier, $\tau$ the mean free time between collisions (or the mean relaxation time of the band state), and $m$ the effective mass of the charge carrier. The relaxation time due to scattering processes induced by the nonlocal coupling is given by[21]

$$\frac{\hbar}{\tau} \propto \frac{L}{t^{(0)}} k_B T \tag{12}$$

Consideration of eq 12 suggests that in pentacene, where $L/t^{(0)} < 0.1$ (see Table 10), the interaction with optical phonons is unable to wipe out a band-like mechanism, even around room temperature. Indeed, the energy uncertainty in the band states ($\hbar/\tau$) due to the scattering processes around room temperature is about 3 meV, which is much smaller than the transfer integrals (and thus the electronic band widths) in this crystal. In the case of naphthalene, $L/t^{(0)}$ can be closer to unity (see Table 9); as a result, the models based on the relaxation-time approximation are expected to become in general inadequate.

It is important to note that, in addition to the scattering processes that work toward decreasing the carrier mobility, the nonlocal coupling also leads to a phonon-assisted contribution to the mobility.[57,58] The origin of the phonon-assisted term can be easily understood in the case where charge transport proceeds in the hopping regime via uncorrelated jumps of localized charge carriers. Assuming that these hops can be described as a self-exchange electron transfer from a charged (and relaxed) molecule to a nearby neutral molecule, the carrier mobility is expressed as[59]

$$\mu = \frac{qd^2}{k_B T} k_{ET} \tag{13}$$

Here, $k_{ET}$ denotes the electron-transfer rate and $d$ the distance between molecules. In the semiclassical nonadiabatic limit, the Marcus electron-transfer (hopping) rate is given by[59]

$$k_{ET} = \frac{t^2}{\hbar}\sqrt{\frac{\pi}{\lambda k_B T}} \exp\left[-\frac{(\Delta G + \lambda)^2}{4\lambda k_B T}\right] \tag{14}$$

where $\Delta G$ is the free energy of the electron-transfer reaction.

It is worth stressing that the conventional Marcus-type theories usually apply the Condon approximation where the transfer integrals do not depend on the reaction coordinates; thus, they *do not account* for the nonlocal vibrational coupling. The nonlocal coupling can be introduced by making the following substitution in eq 14:[60]

$$t^2 \Rightarrow \langle t^2 \rangle = (t^{(0)})^2 + \sigma^2 \tag{15}$$

The phonon-assisted contribution, i.e., the second term in eq 15, arises due to the effective increase in the squared transfer integrals because of the nonlocal coupling mechanism.[57] (Note that eq 15 is based on the assumption of linear electron−vibration interactions, which is the case we have considered here; for a more general description, see ref 61.) Our results again indicate that the phonon-assisted contribution is largest in the naphthalene crystal and smallest in the pentacene crystal. However, it is important to underline that, due to its dual nature, the actual impact of the nonlocal vibrational coupling on charge transport can be accurately obtained only in the framework of a proper polaron model. (We have now started to investigate this issue on the basis of a semiclassical model and the results will be discussed elsewhere.)

## 4. Conclusions

We have used DFT and MM approaches to characterize the interaction between holes or electrons and optical phonons in oligoacene crystals. The results demonstrate that, in the naphthalene and anthracene crystals, the strength of the nonlocal electron−phonon couplings is comparable to the strength of the electronic couplings. Therefore, these systems can be appropriately described neither in the weak nor in the strong electronic coupling limit. In contrast, the nonlocal electron−phonon couplings in tetracene and pentacene are found to be significantly smaller than the electronic couplings (band widths); the strong electronic coupling limit appears thus to be adequate for these crystals.

The calculations point to a decrease in the relaxation energy associated with the nonlocal electron−phonon coupling with the size of the molecule. Holes and electrons in oligoacenes are coupled to both inter- and intramolecular vibrations; the relative contribution of the low-frequency (essentially *inter*molecular) phonons to the nonlocal coupling increases with the molecule size, while the contribution of high-frequency phonons decreases. At this point, it is not clear whether these trends are general and reflect an intrinsic physical property of organic semiconductors or are specific to the oligoacene molecular crystals. Investigation of the nonlocal couplings in other families of organic molecular crystals and extension of the current work

(57) Gosar, P.; Choi, S. I. *Phys. Rev.* **1966**, *150*, 529.
(58) Gosar, P.; Vilfan, I. *Mol. Phys.* **1970**, *18*, 49.
(59) Pope, M.; Swenberg, C. E.; Pope, M. *Electronic processes in organic crystals and polymers*, 2nd ed.; Oxford University Press: New York, 1999.
(60) Beratan, D. N.; Skourtis, S. S.; Balabin, I. A.; Balaeff, A.; Keinan, S.; Venkatramani, R.; Xiao, D. Q. *Acc. Chem. Res.* **2009**, *42*, 1669.
(61) Medvedev, E. S.; Stuchebrukhov, A. A. *J. Chem. Phys.* **1997**, *107*, 3821.

to account for phonon dispersion and contributions from acoustical modes are currently under way.

**Acknowledgment.** This work was primarily supported by the National Science Foundation under the MRSEC Program (Award DMR-0819885) and by the Office of Naval Research.

**Supporting Information Available:** Force field parameters used in the MM simulations and the unit-cell atomic coordinates of oligoacene crystals; complete lists of the MM and DFT frequencies and vibrations couplings for the naphthalene, anthracene, tetracene, and pentacene molecular crystals; MM-calculated eigenvectors in tetracene; contributions of the low- and high-frequency phonons for electrons in the oligoacene molecular crystals; size dependence of the *G* parameter in oligoacenes; and complete ref 38. This information is available free of charge via the Internet at http://pubs.acs.org.

JA1040732